Journal of Power Sources 242 (2013) 604–609

Contents lists available at SciVerse ScienceDirect

Journal of Power Sources

journal homepage: www.elsevier.com/locate/jpowsour

Short communication

A general polymer-assisted solution approach to grow transition metal oxide nanostructures directly on nickel foam as anodes for Li-ion batteries

Yun Xu [a], Ling Fei [a], Engang Fu [b], Bin Yuan [a], Joshua Hill [a], Yingxi Chen [a], Shuguang Deng [a], Paul Andersen [a], Yongqiang Wang [c], Hongmei Luo [a,*]

[a] Department of Chemical Engineering, New Mexico State University, NM 88003, United States
[b] State Key Laboratory of Nuclear Physics and Technology, School of Physics, Peking University, Beijing 100871, China
[c] Materials Science and Technology Division, Los Alamos National Laboratory, Los Alamos, NM 87545, United States

HIGHLIGHTS

- Co_3O_4 were grown on nickel foam by polymer-assisted solution method.
- Carbon left from decomposition of polymer is an active binder between Co_3O_4 and nickel foam.
- Co_3O_4 on nickel foam showed much improved battery performance.

ARTICLE INFO

Article history:
Received 29 January 2013
Received in revised form
15 May 2013
Accepted 23 May 2013
Available online 8 June 2013

Keywords:
Lithium-ion battery
Co_3O_4
Carbon
Anode

ABSTRACT

Cobalt oxide nanostructures have been successfully grown on nickel foam by a facile polymer-assisted chemical solution method for lithium-ion battery anodes. The carbon left from the decomposition of polymers is an effective binder between the metal oxides and nickel foam. As compared to the metal oxide powder prepared in a conventional way by using polymer binder and carbon black, these one-step direct growth electrodes showed much better Li storage properties with high capacities, stable cyclability, and rate capability: Co_3O_4 on nickel foam gave a capacity of 900 mAh g^{-1} at a current density of 1 A g^{-1} and 600 mAh g^{-1} at 4 A g^{-1}. The good performances of these electrodes could be attributed to intimate contact between the active material and nickel foam, the porosity of the current collector, and the network structure of the active materials. This general method could also be applied to other transition metal oxides.

1. Introduction

Anode materials with both high specific energy densities and good rate capabilities are desirable for lithium-ion batteries intended for use in hybrid electric vehicles (HEVs) and plug-in hybrid electric vehicles (PHEVs). To achieve high power density and energy density, the electrochemical activity and kinetics of the electrodes are the dominant factors. It has been proven that it is effective to enhance the kinetics of ions and electrons transport in electrode–electrolyte and at the electrode–current collector interface [1–3]. Currently, the general preparation method of electrodes involves using an insulating poly(vinylidene difloride) as binder and carbon black as a conductive additive, both of which add extra weight to the electrodes and decrease their overall specific capacity. In addition, the polymer binder greatly decreases the electrical conductivity of the electrode materials, and introduces additional interfaces of active material/polymer binder and active material/active material. By directly growing one-dimensional (1D) or two-dimensional (2D) nanostructures on the current collector substrates, the extra weight of polymer binder and carbon black and their undesirable interfaces are eliminated; therefore, the specific capacity of the electrodes is improved [4–10]. Efficient electron transport and fast Li^+ diffusion are achieved because there is no insulating polymer binder to prevent intimate contact between the active material and current collector. For example, $FeVO_4$ nanosheet arrays directly grown on stainless steel foil delivered a

* Corresponding author. Tel.: +1 575 646 4204; fax: +1 575 646 7706.
E-mail addresses: hluo@nmsu.edu, luohongmeitulane@yahoo.com (H. Luo).

0378-7753/$ – see front matter © 2013 Elsevier B.V. All rights reserved.
http://dx.doi.org/10.1016/j.jpowsour.2013.05.116

stable capacity even at a high current density of 20 A g^{-1} [11]. Iron oxide nanorod arrays grown on the titanium substrate showed a higher reversible capacity compared to the iron oxide powders [7].

Transition metal oxides (TMOs) have been considered as promising anode candidates for their high capacity (e.g. >600 mAh g^{-1}). However, due to poor conductivity, TMOs are always synthesized as nanostructure and coupled with conductive carbon when applied in lithium-ion batteries [4,12–21]. By growing TMOs directly on the surface of nickel foam current collector, the porous structure of nickel foam will promote the diffusion of electrolyte and maximize the utilization of active material. Many efforts have been put on the direct growth of TMOs on nickel foam for energy storage [9,22,23]. Although the performances of these electrodes are impressive, the synthesis processes are always tedious or not able to achieve large-scale production. Compared to those complicated and high cost methods, developing a facile and general strategy to synthesize the binder free electrode is of great importance. In this paper, we report a general polymer-assisted chemical solution method for synthesizing TMOs nanostructure directly on nickel foam (cobalt oxide in this paper, nickel oxide in the supporting information). Polyethylenimine (PEI)/ethylenediaminetetraacetic acid (EDTA) and polyvinylpyrrolidone (PVP) were tried as the polymers to demonstrate the feasibility of this method.

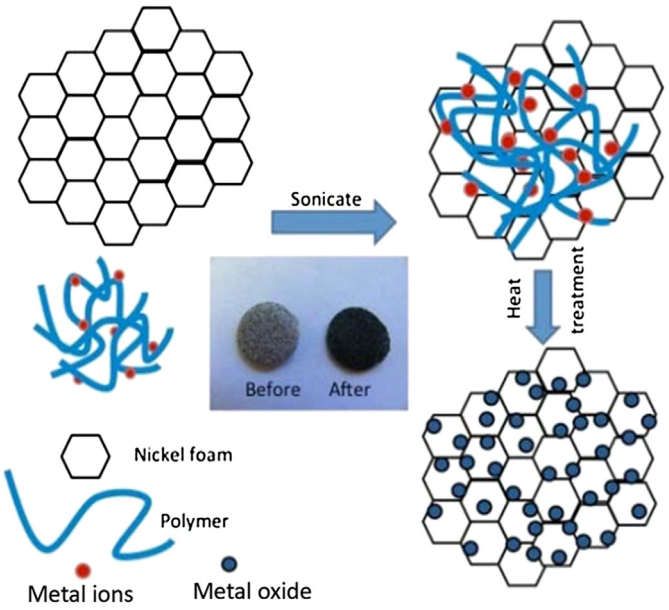

Scheme 1. Schematic mechanism for the growth process of TMOs on nickel foam. The original nickel foam (before) and Co_3O_4 covered on nickel foam (after) are photographed.

2. Experimental

The simple polymer-assisted chemical solution synthesis process is described as following. A viscous cobalt-polymer solution was prepared by dissolving cobalt nitrate (1 g), PEI (2 g, 50 wt% PEI in water), and EDTA (1 g) in 10 mL deionized water, or cobalt nitrate (1 g) and PVP (1 g) were dissolved in 10 mL deionized water. The polymers function as binding agents to metal ions and increase the viscosity of the solution. The nickel foam was sonicated in the mixture solution for 2 min to make sure that all the skeleton of nickel foam was covered by precursor solution, then taken out and transferred to a crucible boat in a box furnace. The nickel foam with cobalt-polymer solution was heated at 150 °C for 1 h and 450 °C for 3 h. Cobalt oxide directly grown on nickel foam was used as anodes after sonication to remove extra oxide powders from the surface of nickel foam.

3. Results and discussion

3.1. Structure and morphology characterization

The structure and morphology of the as-prepared samples were characterized by X-ray diffraction (XRD; MMA GBC, Cu Kα, radiation), field emission scanning electron microscopy (FESEM; JEOL-7500, 2 keV), and transmission electron microscopy (TEM; FEI Tecnai, 300 keV). Thermogravimetric analysis was performed Pyris 1 TGA thermogravimetric analyser (Perkin Elmer). Electrochemical measurements were carried out using CR-2032 coin cells. For the preparation of the working electrode, cobalt oxide on nickel foam was directly used as electrode. A lithium foil was used as the counter electrode. A solution of 1 M $LiPF_6$ in ethylene carbonate (EC)/dimethyl carbonate (DMC) (1:1 in volume) was used as the electrolyte. Galvanostatic cycling was performed using a Land battery testing system. In a control experiment, Co_3O_4 powder (without nickel foam) was prepared by heating the cobalt nitrate with EDTA and PEI mixture solution at 150 °C for 1 h and 450 °C for 3 h. Co_3O_4 powder was used to prepare the electrode in a conventional way, which employs polymer binder and carbon black with active material/polymer binder/carbon mass ratio of 70:10:20.

The growth mechanism of TMOs on nickel foam is presented in Scheme 1. The polymers here serve as a binder in the synthesis process. During the immersing process, the long polymer chains tangle the nickel foam and fixed the metal ions on the skeleton. The polymers not only help connect the metal ions stick to the nickel foam but also determine the nanostructure of the metal oxide formed after annealing process as discussed later in this paper. Due to the incomplete decomposition of polymer at 450 °C, residual carbon acts as an effective binder between the metal oxides and nickel foam.

XRD was employed to confirm the formation of TMOs. A typical XRD pattern of the Co_3O_4 is shown in Fig. 1. The XRD pattern matches well with the standard crystallgraphic spectrum of spinel Co_3O_4 (JCPDS No.43-1003), indicating a successful growth of Co_3O_4. It is noted that the XRD pattern for Co_3O_4 has no difference from two different polymers.

SEM images of Co_3O_4 prepared from PEI and EDTA are presented in Fig. 2a and b (a higher magnification of the square area in red in Fig. 2a). As compared with the original nickel foam (inset of Fig. 2b), we found that the Co_3O_4 sheet on nickel foam keeps the same skeleton shape as the nickel foam, and the skeleton of nickel

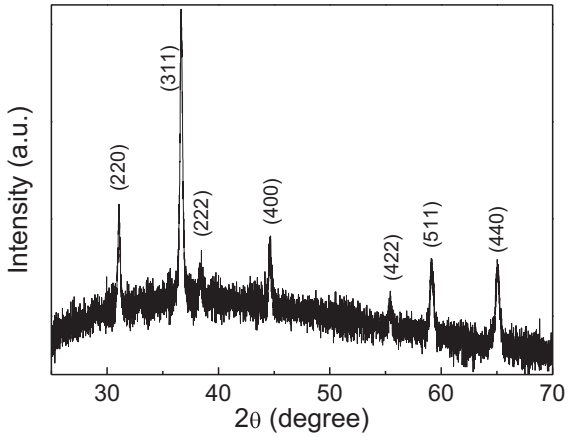

Fig. 1. XRD patterns of Co_3O_4.

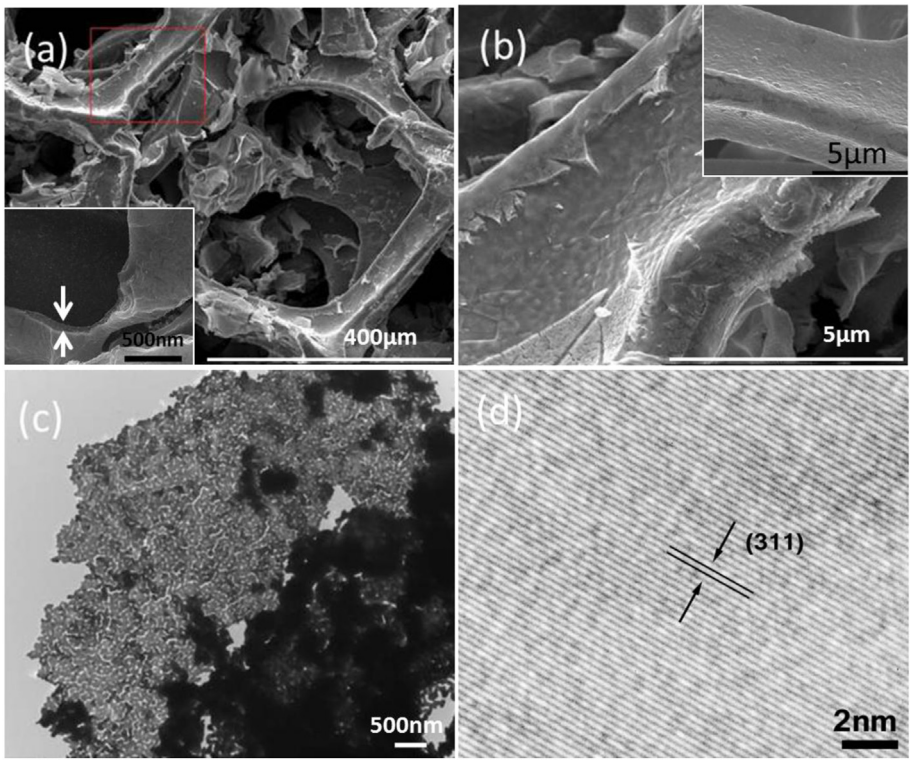

Fig. 2. (a) SEM image of Co_3O_4 on nickel foam prepared from PEI and EDTA, the inset is the cross-section of Co_3O_4 sheet; (b) A higher magnification of the SEM image of the square area in red in (a), the inset is the original nickel foam; (c) TEM image; and (d) High resolution TEM image of Co_3O_4 scratched from nickel foam. (For interpretation of the references to colour in this figure legend, the reader is referred to the web version of this article.)

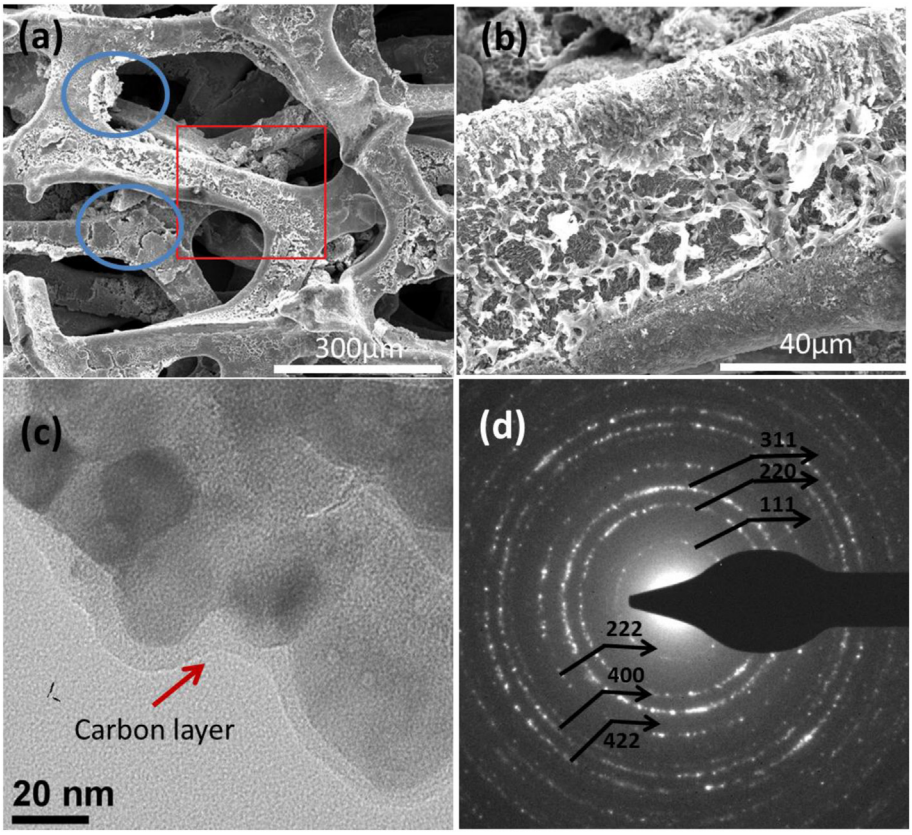

Fig. 3. (a) SEM image of Co_3O_4 on nickel foam prepared from PVP; (b) A higher magnification of SEM image of the square area in red in (a); (c) TEM image, and (d) Electron diffraction pattern of Co_3O_4 scratched from nickel foam. (For interpretation of the references to colour in this figure legend, the reader is referred to the web version of this article.)

foam is all covered with Co_3O_4 sheet. Co_3O_4 sheet sticks on the surface of nickel foam. The cross-section of the Co_3O_4 sheet, as shown in the inset of Fig. 2a, indicates the thickness of Co_3O_4 of around 100 nm. TEM image in Fig. 2c shows that Co_3O_4 displays network sheet structure, and these sheets overlap each other as demonstrated by the dark area. High resolution TEM image in Fig. 2d shows that the lattice spacing is about 0.246 nm, corresponding to the lattice spacing of the (311) plane for spinel Co_3O_4. We also put nickel foam in an EDTA and PEI polymer solution without cobalt nitrate, or in a cobalt nitrate water solution without polymer, and let them go through the same heat treatment. However, nothing was accumulated on the nickel foam after sonication, indicating that the polymer helps the formation of Co_3O_4 network.

Fig. 3a and b presents the morphology of Co_3O_4 nanostructure prepared from PVP. Nickel foam is also covered completely by Co_3O_4. Some Co_3O_4 particles form aggregation as shown in the blue area in Fig. 3a. Further sonication could remove these aggregations. TEM image in Fig. 3c reveals that Co_3O_4 are composed of nanoparticles with diameter of around 30 nm. Carbon layers are observed on these particles. As shown in Figure S1 (in supporting information), TGA result shows that around 5 wt% of carbon left in the product. The carbon left after the decomposition of polymer is an effective binder between Co_3O_4 and nickel foam. The interconnected structure provides a continuous pathway for lithium ions during charge and discharge. Electron diffraction pattern in Fig. 3d matches well with the XRD results.

3.2. Electrochemical characterization

The assembled Co_3O_4 on nickel foam/Li half-cells were tested by galvanostatic charge and discharge in a voltage range of 0.005–3 V (vs. Li^+/Li). Fig. 4a–d presents electrochemical performance of Co_3O_4 on nickel foam prepared from PEI and EDTA. Fig. 4a shows the rate performance of the Co_3O_4 on nickel foam at various current densities. Mass loading of Co_3O_4 on nickel foam was 4 mg cm^{-2} for the cell used for rate performance test. The electrode delivered a high capacity above 900 mAh g^{-1} (estimated volumetric capacity of 450 mAh cm^{-3} from the calculation of specific capacity, mass loading, and thickness of Ni foam of 80 μm) at current density of 1 A g^{-1} (~1 C), 830 mAh g^{-1} at 2 A g^{-1}, and 600 mAh g^{-1} at 4 A g^{-1}.

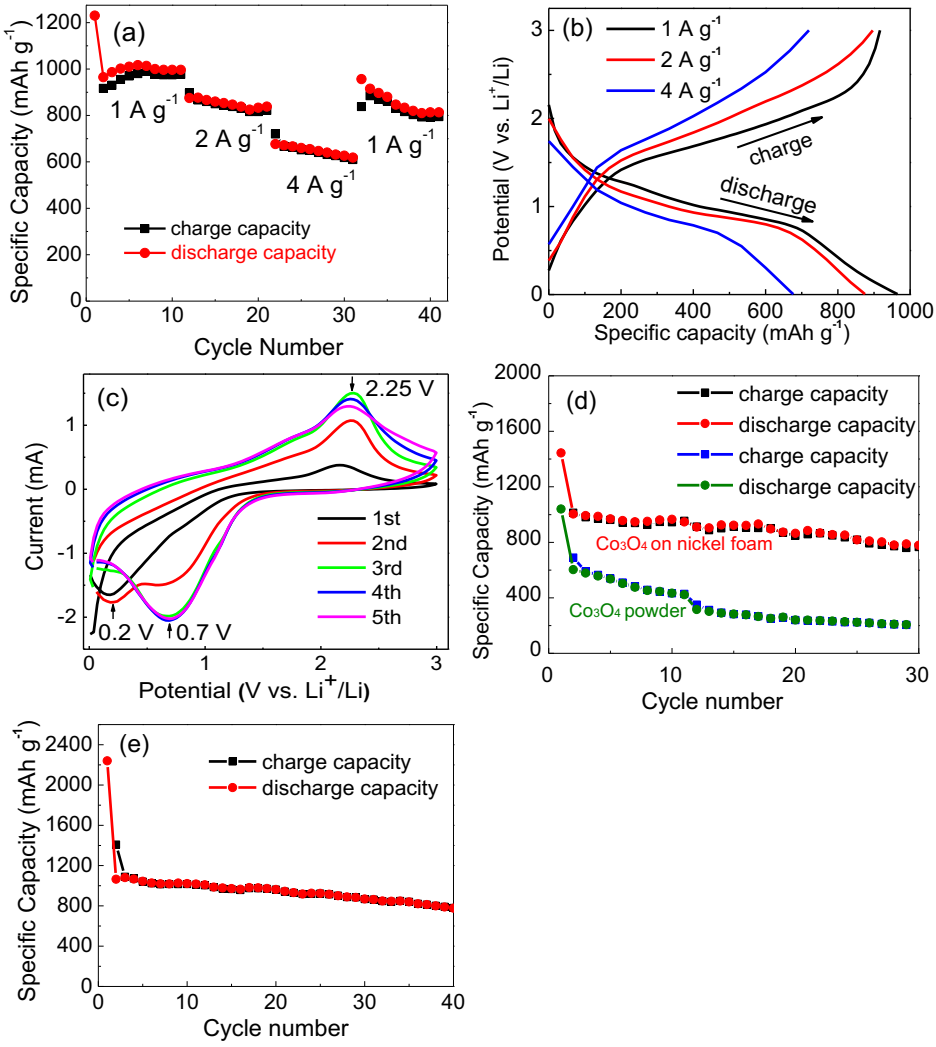

Fig. 4. Electrochemical performance of Co_3O_4 on nickel foam: (a) Rate performance of Co_3O_4 from PEI/EDTA with increasing current density from 1 A g^{-1} to 4 A g^{-1}; (b) Discharge/charge voltage profile of Co_3O_4 from PEI/EDTA at current densities of 1, 2, and 4 A g^{-1}; (c) Cyclic voltammetry of Co_3O_4 from PEI/EDTA at a scan rate of 1 mV s^{-1}; (d) Cycle performance of Co_3O_4 on nickel foam from PEI/EDTA and Co_3O_4 powders at a current density of 1 A g^{-1}; and (e) Cycle performance of Co_3O_4 on nickel foam from PVP at a current density of 1 A g^{-1}.

The capacity was recovered to 800 mAh g^{-1} when the current density was changed back to 1 A g^{-1}, with a retention rate of 88.9%, demonstrating that the structure of electrode was not dramatically changed when cycled at a high current density. Fig. 4b illustrates the charge and discharge profile at different current densities of 1, 2 and 4 A g^{-1}. The plateau is still distinguished even at a high current density of 4 A g^{-1} as well as it is at a low current density of 1 A g^{-1}, indicating that the fast charge transport occurs in the electrodes and across the interface between the electrode and current collector.

Fig. 4c presents cyclic voltammograms (CV) of Co_3O_4 on nickel foam. The cyclic voltammetry was performed in the potential range of 0.005–3 V (vs. Li^+/Li) at a scan rate of 1 mV s^{-1}. In the first cycle, a cathodic peak at 0.2 V corresponds to an electrochemical reduction (lithiation) reaction of Co_3O_4 with Li. The observed anodic peak at 2.25 V for Co_3O_4 is ascribed to the oxidation (delithiation) reaction of Co_3O_4. The formation of Co and Li_2O and the re-formation of Co_3O_4 can be described by the following electrochemical conversion reaction [4,24,25]:

$$Co_3O_4 + 8Li^+ + 8e^- \leftrightarrow Co + 4Li_2O$$

The cathodic peak shifted to 0.7 V in the second cycle, which corresponds to the lithiation process and the decomposition of electrolyte and formation of a solid electrolyte interface (SEI). The peak intensity increases from the first cycle through the third cycle and remains almost the same for the subsequent cycles. The increased peak intensity in the first three cycles may result from the activation of the electrode and penetration of the electrolyte into the porous nickel foam. In later cycles, the peak intensity remains the same, indicating the excellent reversibility and stability of the electrode material.

Fig. 4d presents the cycle performance of the Co_3O_4 on nickel foam at 1 A g^{-1}. Mass loading for the Co_3O_4 on nickel foam is 6 mg cm^{-2}. The discharge capacity at the 1st, 2nd, 10th and 30th cycles is 1444, 1004, 965, 778 mAh g^{-1}, respectively, with the irreversible capacity of 440 mAh g^{-1} (the difference between the 1st discharge and charge capacities), which results from the formation of SEI [12,26,27]. The battery performance of Co_3O_4 directly grown on nickel foam is much better than the Co_3O_4 powders prepared in a conventional way by using polymer binder and carbon black. For example, at the current density of 1 A g^{-1}, the discharge capacity of Co_3O_4 powder at the 1st, 2nd and 10th cycles is 1040, 603, and 434 mAh g^{-1}, respectively. The Co_3O_4 on nickel foam electrode showed much higher discharge capacity, demonstrating the superiority of the direct growth method. In the sample prepared in a conventional way, active material can't be fully used because of blockage by the polymer binder. In contrast, Co_3O_4 prepared by the direct growth method provides an intimate contact between the Co_3O_4 and the nickel current collector, which enhances the migration of lithium ions and electrons. Furthermore, the active material prepared is distributed on the surface of porous nickel foam with a higher surface area where electrochemical reactions can occur.

Same galvanostatic charge and discharge were tested for Co_3O_4 on nickel foam prepared from PVP. Mass loading was around 6 mg cm^{-2}. The cycle performance is shown in Fig. 4e at a current density of 1 A g^{-1}. The 1st discharge capacity is 2240 mAh g^{-1} and the charge capacity is 1410 mAh g^{-1}, resulting in a larger irreversible capacity of 830 mAh g^{-1}. Co_3O_4 delivered a capacity of 780 mAh g^{-1} after 40 cycles. Both Co_3O_4 prepared from PEI/EDTA and PVP delivered comparable capacities, except that Co_3O_4 from PVP has a larger irreversible capacity. The higher the surface area is, the more irreversible reaction takes place. Co_3O_4 from PVP has a smaller particle size, therefore, it may have larger surface area. The capacity loss of the cells along cycles could be attributed to the loose contact between metal oxide aggregations and nickel foam. Nevertheless, results are better than most of the previous reported Co_3O_4 nanostructures and composites [21,26–30].

4. Conclusion

In summary, we have developed a facile polymer-assisted chemical solution method to grow TMOs nanostructure directly on nickel foam. The resulting TMOs can be directly used as Li-ion battery anodes without an addition of any ancillary materials. Co_3O_4 nanostructure grown on nickel foam prepared from PEI and EDTA delivered a capacity of 600 mAh g^{-1} even at current density of 4 A g^{-1}. The one-step obtained electrodes showed very good Li storage properties with high capacities, stable cyclability and excellent rate capability, which attributed to the short diffusion length between the active material and current collector and the porosity of the current collector.

Acknowledgments

Hongmei Luo acknowledges the funding support from NSF under Grant No. 1131290, New Mexico Consortium and Los Alamos National Laboratory. Specifically, Yun Xu and materials characterization were supported by New Mexico Consortium and Los Alamos National Laboratory. Ling Fei, Joshua Hill, Yingxi Chen, and materials systems were supported by NSF.

Appendix A. Supplementary data

Supplementary data related to this article can be found at http://dx.doi.org/10.1016/j.jpowsour.2013.05.116.

References

[1] S.K. Cheah, E. Perre, M. Rooth, M. Fondell, A. Hårsta, L. Nyholm, M. Boman, T. Gustafsson, J. Lu, P. Simon, K. Edström, Nano Lett. 9 (2009) 3230–3233.
[2] K.F. Chen, S.Y. Song, D.F. Xue, Cryst. Eng. Commun. 15 (2013) 144–151.
[3] L. Zheng, Y. Xu, D. Jin, Y. Xie, J. Mater. Chem. 20 (2010) 7135–7143.
[4] X.Y. Xue, S. Yuan, L.L. Xing, Z.H. Chen, B. He, Y.J. Chen, Chem. Commun. 47 (2011) 4718–4720.
[5] J. Jiang, J.H. Zhu, Y.M. Feng, J.P. Liu, X.T. Huang, Chem. Commun. 48 (2012) 7471–7473.
[6] Q.W. Wang, X.B. Liu, G. Yu, X. Hou, D. Chen, G. Shen, J. Mater. Chem. A (2013).
[7] Y.Q. Song, S.S. Qin, Y.W. Zhang, W.Q. Gao, J.P. Liu, J. Phys. Chem. C 114 (2010) 21158–21164.
[8] X. Chen, N.Q. Zhang, K.N. Sun, J. Mater. Chem. 22 (2012) 15080–15084.
[9] S.B. Ni, X.L. Yang, T. Li, J. Mater. Chem. 22 (2012) 2395–2397.
[10] X. Chen, K.N. Sun, E.S. Zhang, N.Q. Zhang, RSC Adv. 3 (2013) 432–437.
[11] D. Sim, X.H. Rui, J. Chen, H.T. Tan, T.M. Lim, R. Yazami, H.H. Hng, Q.Y. Yan, RSC Adv. 2 (2012) 3630–3633.
[12] Y.Z. Su, S. Li, D.Q. Wu, F. Zhang, H.W. Liang, P.F. Gao, C.W. Cheng, X.L. Feng, ACS Nano 6 (2012) 8349–8356.
[13] H. Chen, S.X. Zhou, M. Chen, L.M. Wu, J. Mater. Chem. 22 (2012) 25207–25216.
[14] H.L. Wang, H.S. Casalongue, Y. Liang, H.J. Dai, J. Am. Chem. Soc. 132 (2010) 7472–7477.
[15] Y.G. Li, H.L. Wang, L.M. Xie, Y.Y. Liang, G.S. Hong, H.J. Dai, J. Am. Chem. Soc. 133 (2011) 7296–7299.
[16] H.L. Wang, L.F. Cui, Y. Yang, C.H. Sanchez, J.T. Robinson, Y. Liang, Y. Cui, H.J. Dai, J. Am. Chem. Soc. 132 (2010) 13978–13980.
[17] G.M. Zhou, D.W. Wang, F. Li, L.L. Zhang, N. Li, Z.S. Wu, L. Wen, G.Q. Lu, H.M. Cheng, Chem. Mater. 22 (2010) 5306–5313.
[18] Y.Q. Zou, J. Kan, Y. Wang, J. Phys. Chem. C 115 (2011) 20747–20753.
[19] X.Y. Zhao, M.H. Cao, C.W. Hu, RSC Adv. 2 (2012) 11737–11742.
[20] C.Z. Yuan, L. Yang, L.R. Hou, L.F. Shen, F. Zhang, D.K. Li, X.G. Zhang, J. Mater. Chem. 21 (2011) 18183–18185.
[21] S.A. Needham, G.X. Wang, H.K. Liu, J. Power Sources 159 (2006) 254–257.
[22] C. Guan, J. Liu, C.W. Cheng, H.X. Li, X.L. Li, W.W. Zhou, H. Zhang, H.J. Fan, Energy Environ. Sci. 4 (2011) 4496–4499.

[23] Y.Y. Gao, S. Cao, D. Cao, G. Wang, J. Yin, J. Power Sources 195 (2010) 1757–1760.
[24] Z.S. Wu, W.C. Ren, L. Wen, L.B. Gao, J.P. Zhao, Z.P. Chen, G.M. Zhou, F. Li, H.M. Cheng, ACS Nano 4 (2010) 3187–3194.
[25] N. Yan, L. Hu, Y. Li, Y. Wang, H. Zhong, X.Y. Hu, X.K. Kong, Q.W. Chen, J. Phys. Chem. C 116 (2012) 7227–7235.
[26] R. Mukherjee, A.V. Thomas, A. Krishnamurthy, N. Koratkar, ACS Nano 6 (2012) 7867–7878.
[27] A.L.M. Reddy, A. Srivastava, S.R. Gowda, H. Gullapalli, M. Dubey, P.M. Ajayan, ACS Nano 4 (2010) 6337–6342.
[28] L. Zhan, Y.L. Wang, W.M. Qiao, L.C. Ling, S.B. Yang, Electrohcim. Acta 78 (2012) 440–445.
[29] D.K. Su, W.S. Kim, G. Wang, Chem. Eur. J. 18 (2012) 8224–8229.
[30] X.H. Wang, X.W. Li, X.L. Sun, F. Li, Q.M. Liu, Q. Wang, D.Y. He, J. Mater. Chem. 21 (2011) 3571–3573.